Biomaterials 84 (2016) 241–249

Contents lists available at ScienceDirect

Biomaterials

journal homepage: www.elsevier.com/locate/biomaterials

Synthesis and comparative evaluation of novel ^{64}Cu-labeled high affinity cell-specific peptides for positron emission tomography imaging of tumor vasculature

Joseph R. Merrill [a], Krzysztof Krajewski [b], Hong Yuan [a], Jonathan E. Frank [a], David S. Lalush [a, c], Cam Patterson [d], Anka N. Veleva [c, e, *]

[a] Biomedical Research Imaging Center, University of North Carolina, Chapel Hill, NC 27599, USA
[b] Department of Biochemistry and Biophysics, University of North Carolina, Chapel Hill, NC 27599, USA
[c] Department of Biomedical Engineering, North Carolina State University, Raleigh, NC 27695, USA
[d] NewYork Presbyterian Hospital, Weill Cornell Medical Center, New York, NY 10065, USA
[e] Department of Chemical and Biomolecular Engineering, North Carolina State University, Raleigh, NC 27695, USA

ARTICLE INFO

Article history:
Received 14 October 2015
Received in revised form
31 December 2015
Accepted 15 January 2016
Available online 21 January 2016

Keywords:
Molecular imaging
Tumor angiogenesis
^{64}Cu-labeled cell-specific peptides
Diagnostic PET radiopharmaceuticals
Radiation absorbed dose

ABSTRACT

Tumor angiogenesis, the formation of new tumor blood supply, has been recognized as a hallmark of cancer and represents an important target for clinical management of various angiogenesis-dependent solid tumors. Previously, by screening a bacteriophage peptide library we have discovered the FHT-peptide sequence that binds specifically to bone marrow-derived tumor vasculature with high affinity. Here in an effort to determine the potential of the FHT-peptide for in vivo positron emission tomography (PET) imaging of aggressive tumor vasculature we studied four FHT-derivatives: NOTA-FHT, NOTA-(FHT)2, NOTA-PEG-FHT, and NOTA-PEG-(FHT)2. These peptide analogs were synthesized, labeled with the PET radionuclide ^{64}Cu, and characterized side-by-side with small animal PET and computed tomography imaging (microPET/CT) at 1 h, 4 h, and 24 h post injection in a subcutaneous Lewis lung carcinoma (LLC) tumor model. Because of its excellent in vivo kinetic properties and high tumor-to-background ratio, the ^{64}Cu-NOTA-FHT radiopeptide was selected for more detailed evaluation. Blocking studies with excess of unlabeled peptide showed specific and peptide mediated ^{64}Cu-NOTA-FHT tumor uptake. Biodistribution experiments in the same tumor model confirmed microPET/CT imaging results. Human radiation absorbed dose extrapolated from rodent biodistribution of ^{64}Cu-NOTA-FHT revealed favorable dosimetry profile. The findings from this investigation warrant further development of ^{64}Cu-NOTA-FHT as a potential targeted diagnostic radiopharmaceutical for PET imaging of aggressive tumor vasculature.

1. Introduction

Biomaterials play an essential role in a variety of diagnostic and therapeutic procedures and perform functions to direct and control interactions with living systems that have crucial effects on overall biological performance and clinical outcomes of these procedures [1]. In most instances highly specific interactions have been regarded as key features in biomaterials design improving biocompatibility and recapitulating material-cell specific interactions [2,3]. For example, the short Arg-Gly-Asp (RGD) tripeptide, the minimal sequence for binding to integrin receptors, has been widely utilized to impart biological function to synthetic materials and facilitate material-cell recognition events [4–9]. With recent advances in combinatorial, high throughput screening technologies such as bacreriophage (phage) display, new engineered peptides have been discovered that bind with high affinity to their biologic targets in a highly specific manner [10–14]. Phage display-selected, disease-specific peptides hold promise in precision medicine for use as molecularly targeted diagnostic imaging agents [15–21]. Disease-specific, peptide-based imaging compositions have the potential to extend the clinical utility of conventional

* Corresponding author. Department of Biomedical Engineering, North Carolina State University, Raleigh, NC 27695, USA.
E-mail addresses: joseph_merrill@med.unc.edu (J.R. Merrill), krzysztof_krajewski@med.unc.edu (K. Krajewski), hong_yuan@med.unc.edu (H. Yuan), jonathan_frank@med.unc.edu (J.E. Frank), dslalush@ncsu.edu (D.S. Lalush), cpatters@nyp.org (C. Patterson), anveleva@ncsu.edu (A.N. Veleva).

http://dx.doi.org/10.1016/j.biomaterials.2016.01.031
0142-9612/

imaging techniques such as positron emission tomography (PET) by enabling integration of accurate diagnostics with therapy to achieve better outcomes.

Tumor angiogenesis, the formation of new tumor blood supply, is a hallmark of cancer and is generally associated with aggressive tumor progression and poor patient prognosis. Tumors form new blood capillaries either from pre-existing mature ones or *de novo* by recruiting circulating pro-angiogenic endothelial and hematopoietic precursor cells mobilized from the host bone marrow [22]. Stromal cells of bone marrow origin have been identified in the vasculature of several pre-clinical models [23–26]. In humans, bone marrow-derived endothelial cells have been detected in patients with multiple myeloma [27], breast cancer [28], non-small cell lung cancer [29], and malignant gliomas [30]. Increased levels of immature precursors in the peripheral blood of patients with breast, colon, prostate, head and neck, renal and ovarian cancer have been shown to correlate with aggressive disease [31]. Furthermore, circulating progenitor cells of bone marrow origin have been exploited as a potential biomarker to guide the use of antiangiogenic therapy in cancer patients [32]. Together, these studies suggest that bone marrow-sourced, circulating pro-angiogenic tumor-homing cells actively participate in tumor angiogenesis and represent a promising target for development of novel diagnostic and therapeutic agents with improved tumor selectivity.

Screening of phage display random peptide libraries has emerged as useful and practical approach for the discovery of new peptide ligands that can bind with high affinity and specificity to a variety of targets including angiogenic blood vessels [33]. Innovative methodological selection protocols in the environment of the whole mouse have been developed to allow for improved targeting in vivo [14,34]. Besides the optimized pharmacokinetics and in vivo binding affinity, peptides selected by unbiased phage screens typically display specificity of 10–100 fold for their target over background tissue [11,13]. Because phage display-selected ligands possess suitable pharmacokinetic properties, i.e., high affinity, tumor uptake and specificity, these targeting vectors have been actively pursued as agents for molecular imaging and non invasive tumor phenotyping [10–12,14–19,33]. In addition to good transport properties, and the ability to both penetrate rapidly into solid tumors and recognize hidden or rare epitopes, peptides have in general low toxicity and immunogenicity, and can be produced in large quantities at low cost.

By screening a phage display dodecapeptide library in vivo, we have previously discovered a new amino acid sequence, the FHT-peptide (Phe-His-Thr-Pro-Ser-Gln-Asn-Ser-Ala-Phe-Arg-Leu), that specifically binds with high affinity to bone marrow-derived circulating tumor-homing cells [14]. Unlike the RGD sequence, widely utilized to impart specificity to integrin receptors expressed both on tumor neovasculature and tumor cells, the FHT-peptide selectively binds to a protein expressed on the surface of bone marrow-derived neovascular cells. This unique binding profile of the FHT-peptide provides a novel platform for developing more specific diagnostic and therapeutic agents. Here, we will test the ability of the FHT-peptide, labeled with the ^{64}Cu ($t_{1/2}$ = 12.7 h) positron emitting radionuclide, to selectively target tumor vasculature for in vivo PET imaging. Due to its dual decay characteristics ^{64}Cu (β^+: 17.8%, $E_{\beta+max}$ = 653 keV; β^-: 38.4%, $E_{\beta-max}$ = 578 keV) has promising clinical applications both for diagnostic imaging and targeted radiotherapy. Positron emissions from a ^{64}Cu-labeled peptide radiopharmaceutical will allow the oncologist to obtain diagnostic PET image assessing the malignancy and then provide personalized treatment to the patient using the same ^{64}Cu-radiolabeled composition.

The goal of this study is to identify an FHT-based molecular composition for a PET imaging agent providing the highest ratio of tumor uptake to normal tissue uptake in vivo. Here we report studies that explore the pharmacokinetics and imaging characteristics of four distinct molecular constructs based on the FHT-sequence (Fig. 1) all labeled with the ^{64}Cu radionuclide for PET imaging. FHT-derivatives were prepared with the ^{64}Cu-binding chelate 1,4,7-triazacyclononane 1,4,7-triacetic acid (NOTA). Modifications such as PEGylation and divalent ligand presentation were utilized to modulate in vivo distribution properties of the FHT-compositions. Both approaches, PEGylation and multivalency, are known to modify in vivo pharmacokinetics of small molecules [16,20,21]. FHT-peptide derivatives were prepared using solid phase peptide synthesis protocols, radiolabeled with ^{64}Cu, and characterized side-by-side using dual small animal PET and computed tomography (CT) imaging (microPET/CT) at 1 h, 4 h, and 24 h post injection in a subcutaneous Lewis lung carcinoma (LLC) tumor model. Biodistribution experiments were performed in the same tumor system. Peptide-specific uptake of the lead FHT-composition was demonstrated in blocking studies. Human absorbed doses for the selected lead construct were extrapolated from the rodent biodistribution.

2. Materials and methods

2.1. Reagents and analyses

All chemicals and reagents were of analytical grade or better and were used without further purification. Rink Amide-ChemMatrix resin (loading, 0.52 mmol/g) was purchased from PCAS BioMatrix (Quebec, Canada). 9-Fluorenylmethyloxycarbonyl (Fmoc)-protected standard amino acids, Fmoc-Lys(Fmoc)-OH, Fmoc-Lys(Mtt)-OH, di-tert-butyl dicarbonate (Boc_2O), and the coupling agent 1-[Bis(dimethylamino)methylene]-1H-1,2,3-triazolo[4,5-b] pyridinium 3-oxid hexafluorophosphate (HATU) were purchased from AnaSpec (Freemont, CA). Fmoc-NH-$(PEG)_{12}$-$CH_2CH_2CO_2H$ [1-(9H-fluoren-9-ylmethoxycarbonylamino)-3,6,9,12,15,18,21,24,27,30,33,36-dodecaoxanonatria contan-39-oic acid] was purchased from Quanta Biodesign (Plain City, OH) and p-SCN-Bn-NOTA (2-S-(4-Isothiocyanatobenzyl)-1,4,7-triazacyclononane-1,4,7-triacetic acid) was obtained from Macrocyclics (Dallas, TX). All other solvents and chemicals were purchased from VWR (Atlanta, GA).

The solid phase peptide synthesis was performed on Rink Amide-ChemMatrix resin using PTI Symphony (Protein Technologies, Tuscon, AZ) peptide synthesizer. Analytic high-performance liquid chromatography (HPLC) analyses were performed on a Waters Alliance HPLC system and semi-preparative HPLC purifications were conducted on a Waters 1525 HPLC system. Matrix-assisted laser desorption and ionization time of flight mass spectrometry (MALDI-TOF MS) analysis was carried out using an α-cyano-4-hydroxycinnamic acid matrix on an ABI 4800 mass spectrometer (Sciex, Framingham, MA).

High specific activity ^{64}Cu was obtained from the Washington University School of Medicine (St. Louis, MO) as $^{64}CuCl_2$ in 0.5 M HCl. Copper-64 was produced on a CS-15 biomedical cyclotron by the ^{64}Ni(p,n)^{64}Cu nuclear reaction using previously published methods [35]. All experiments involving the use of radioactive materials were conducted under the authorization of the Radiation Safety Committee at the University of North Carolina – Chapel Hill.

2.2. Peptide synthesis and characterization

Monomeric peptide derivatives were synthesized using 20 μmol of the resin, and dimeric peptide derivatives were synthesized using 12 μmol of the resin. Fmoc-Lys(Mtt)-OH, Fmoc-Lys(Fmoc)-OH,

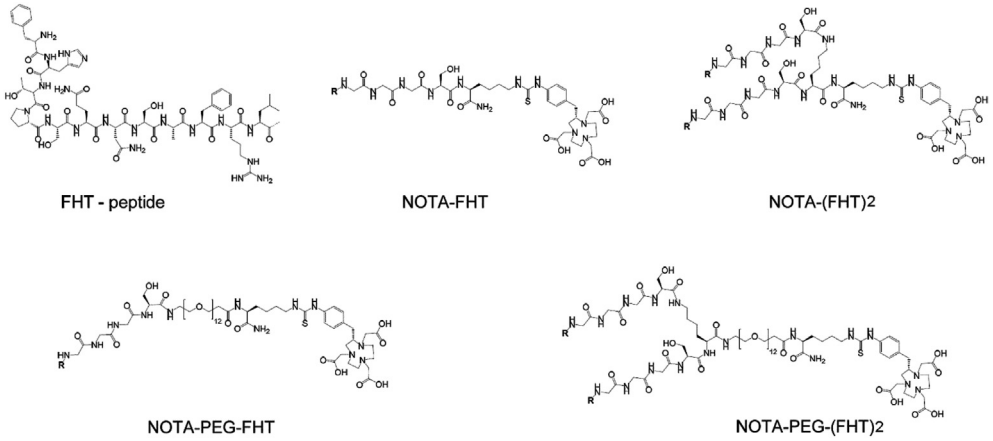

Fig. 1. Chemical structures of FHT-peptide, NOTA-FHT, NOTA-(FHT)2, NOTA-PEG-FHT, and NOTA-PEG-(FHT)2.

and Fmoc-NH-$(PEG)_{12}$-$CH_2CH_2CO_2H$ (PEG) were introduced using single 2 h couplings. The reactions were confirmed by ninhydrin test. All other residues were introduced using double coupling. Fmoc-groups were removed by treatment with 20% piperidine in N,N-dimethylformamide (DMF) followed by washing with DMF. The synthesis of all peptides started with Fmoc-Lys(Mtt)-OH coupling to the resin and Fmoc-group removal. For peptides containing PEG, the residue was introduced by Fmoc-NH-$(PEG)_{12}$-$CH_2CH_2CO_2H$ coupling. Dimeric peptides were synthesized by coupling of Fmoc-Lys(Fmoc)-OH to either Lys(Mtt) or PEG residues and subsequent simultaneous growing of two peptide chains attached to both amine groups of this Lysine residue. After removal of the last Fmoc-group, N-terminal amino groups of all peptides were Boc-protected by mixing with 0.1 mmol Boc_2O and 0.2 mmol N,N-Diisopropylethylamine (DIPEA) in DMF. Mtt protective group was removed by resin treatment with a mixture of 1% trifluoroacetic acid (TFA) and 2% triisopropylsilane (TIPS) in dichlorometane (DCM) followed by washing with DCM, 0.1 M DIPEA in DMF, and DMF. Subsequently, a NOTA group was introduced into the peptides by overnight mixing of peptide-resins with solution of p-SCN-Bn-NOTA (30 μmol) and 0.3 mmol diisopropylethylamine (DIEA) in 0.5 ml DMF. After a reaction was confirmed by ninhydrin test, resin was thoroughly washed with DMF, DCM, methanol (MeOH), and diethyl ether and dried under vacuum overnight. The peptides were cleaved from the resin and deprotected by 2 h treatment with a mixture of 2.5% TIPS, 2.5% water in TFA at room temperature. The crude peptides were precipitated from TFA solution with cold diethyl ether. After centrifugation the peptides were washed 5 times with diethyl ether, air dried, dissolved in 50% acetonitrile (CH3CN) and lyophilized. The crude products were purified by semi-preparative reversed-phase HPLC (Waters Symmetry Shield column, 19 mm × 150 mm, 5 μm, 13 nm, C18), with a 25-min gradient from 15% CH3CN in water (0.1% TFA) to 35% CH3CN in water (0.1% TFA). The flow rate was 5.0 mL/min. Ultraviolet detection was performed at 220 and 270 nm. The homogeneity of the peptides was determined by analytical HPLC (Merck ChromoLith column, 2 mm × 25 mm, 5 μm, 30 nm, RP18e), using a 10 min gradient from 5% CH3CN in water (0.1% TFA) to 25% CH3CN in water (0.1% TFA), at a flow rate of 1 mL/min and ultraviolet detection at 220, and 270 nm. The purity was in the range 73%–95%. The identity of the compounds was confirmed by MALDI-TOF mass spectrometry. Stock solutions from each peptide derivative in PBS (1 g/L) were prepared and aliquots were used for radiolabeling.

2.3. ^{64}Cu – radiolabeling

For each radiolabeling reaction, approximately 2–5 μg of peptide ligand was incubated with 74 MBq $^{64}CuCl_2$ in 0.1 M ammonium acetate buffer (pH 5.5) in a final volume of 200 μl at 50 °C for 30 min. Crude radiolabeled peptide conjugates were purified on Sep-Pack light C18 reversed solid phase extraction cartridges (Waters, Milford, MA) that were pre-conditioned with 1 ml 99.5% ethanol and 5 ml DI water. After passing the reaction mixture through the cartridge, free ^{64}Cu and any impurities were washed with 1 ml DI water and the purified product was eluted from the column with 1 ml 85% ethanol. The solvent was evaporated and the solid residue was reconstituted in phosphate buffered saline (PBS) and filter sterilized immediately before injecting into the mice.

2.4. Cell culture and animal model

Murine Lewis lung carcinoma (LLC) cell line was obtained from ATCC (American Type Culture Collection, Manassas, VA). The LLC cells were grown in high glucose Dulbecco's modified Eagles medium (DMEM) (Gibco/Life Technologies, Grand Island, NY) supplemented with 10% fetal bovine serum (Gibco/Life Technologies). Cells were maintained at 37 °C in a 5% CO_2 humidified incubator. Sub-culturing was performed using standard procedures.

Five to 6-week-old, immunocompetent C57BL/6J female mice were obtained from Jackson Laboratories (Bar Harbor, ME). The mice were supplied food and water *ad libitum* and were used within two weeks following initial acclimation. To establish tumors, mice were anesthetized by intraperitoneal administration of 0.2 M Avertin (approx. 0.2 ml per mouse). LLC cells were trypsinized, washed three times in DMEM, counted, and the concentration of the cell suspension was adjusted to 2×10^6 cells/ml. Approximately 5×10^5 LLC cells (250 μl) were mixed 1:1 with growth factor reduced Matrigel basement membrane matrix (BD Biosciences, Bedford, MA) for a total volume of 500 μl. The cell formulation was injected subcutaneously (s.c.) via a 22-gauge needle in the right inguinal region of each mouse. Solid tumors were established over a period of seven days, resulting in mice with approximately 0.6 cm^3-sized tumors for all experiments. The formula, tumor volume = a × b × b/2, where a and b are the longest and the shortest perpendicular dimensions of the tumor, was used to calculate tumor volumes.

2.5. Small animal PET/CT imaging and analysis

MicroPET and microCT images were acquired on an eXplore Vista small animal PET/CT scanner (GE Healthcare) with center resolution of 1.2 mm and a 46 mm axial field of view. At seven days post-implantation, mice bearing s.c. LLC tumors were anesthetized with 3% isoflurane/air mixture (v/v) and injected intravenously (i.v.) via a catheter into the tail vein with approximately 7.5 MBq radiolabeled peptide at a volume of 150 μl (n = 3 for each condition). After radiopeptide administration the animals were allowed to wake up and resume normal husbandry. At 1 h, 4 h, and 24 h post injection the animal was anesthetized using an isoflurane/air mixture (v/v) (3% for induction and 1.5% for maintenance), placed in a head-first, prone position on a supporting cradle, and advanced into the scanner. The animal's respiratory rate was monitored by a respiratory probe placed underneath the belly, and body temperature was monitored through a rectal temperature probe during imaging. First, a seven-minute CT scan for subsequent attenuation correction and anatomical reference was acquired followed by a static PET scan. All 1 h p.i. and 4 h p.i. emission scans consisted of fifteen-minute signal collection. The 24 h p.i. static PET data were collected for 30 min. In a separate set of experiments binding specificity study was conducted. For these experiments mice were intravenously co-administered radiolabeled peptide together with an excess of unlabeled peptide (20 mg/kg) and microPET/CT images were collected 1 h post-injection.

PET emission data were corrected for decay and dead time, and reconstructed using two dimensional ordered subset expectation maximization (2D-OSEM) algorithms with scatter correction, random correction, and attenuation correction using the manufacturer's proprietary software on the scanner console computer. Data were displayed and analyzed using the AMIDE software (http://www.sourceforge.net/amide). To determine peptide uptake in the tumors, regions of interest (ROI) were manually drawn around the tumor for each scan and the voxels within the ROI with highest radioactivity were quantified by the AMIDE software. ROIs for the liver and kidney were selected in the uniform central regions, placed away from the edges to avoid partial volume effect. ROIs for blood and muscle were drawn around areas of the aorta and on gastrocnemius, respectively. The resulting quantitative data were expressed as percentage of injected dose per gram tissue (%ID/g) which was calculated as %ID/g = activity of interest divided by the injected dose and multiplied by 100%.

2.6. Biodistribution in tumor bearing C57BL/6 mice

Approximately 0.74 MBq of ^{64}Cu-NOTA-FHT in a total volume of 150 μl of saline was injected under anesthesia intravenously via a catheter in the tail vein in LLC tumor-bearing C57BL/6 mice (n = 3 per time point) followed by conscious uptake period of 1 h, 4 h, or 24 h. At each time point mice were sacrificed under anesthesia and blood was immediately collected by cardiac puncture. The liver, kidney, spleen, lungs, heart, stomach, small and large intestines, thyroid, pancreas, bone (femur), muscle and tumor were harvested. The organs were weighed and their radioactivity was measured in an automated gamma counter (WIZARD2, Perkin Elmer Life Sciences, Gaithersburg, MD). Radioactivity concentrations were calibrated, decay-corrected, and expressed as percentage of injected dose per gram tissue (%ID/g).

Tumor uptake and biodistribution of ^{64}Cu-NOTA-FHT were also studied in the presence of unlabeled NOTA-FHT reagent (20 mg/kg) to determine whether accumulation of radioactivity in the tumor is mediated by the targeting peptide. Tumor, blood, and normal tissues were harvested 1 h p.i., radioactivity measured as described above, and reported as %ID/g.

2.7. Dosimetry calculations

The Medical Internal Radiation Dose (MIRD) method [36] was used for estimating the absorbed dose to the following organs: liver, spleen, kidney, lungs, stomach, small and large intestines, thyroid and pancreas. The absorbed dose, with no-cross organ contributions, was calculated following the equation

$$D_k = A_o \times \tau_k \times S$$

where D_k is the mean absorbed dose to organ region k (in Gy); A_o is the administered activity (in Bq), τ_k is the residence time in organ k (in sec), and S is the absorbed dose per cumulated activity (in Gy/Bq.sec). The residence times for each organ were determined based on the assumption of a similar biodistribution of activity versus time in the mouse and the human. Biodistribution data for ^{64}Cu-NOTA-FHT in C57Bl/6 mice at 1 h, 4 h, and 24 h post injection were used to calculate residence times. Physical decay was assumed for activity remaining in organs beyond 24 h. In estimating the internal absorbed doses to human organs, the well established MIRD S-values were used for the absorbed dose of unit cumulated activity for the ^{64}Cu radionuclide [36]. Details of this approach and the corresponding calculations are presented separately in the Data in Brief communication [37].

2.8. Statistical analysis

All quantitative data are reported as mean ± standard deviation (SD) of three independent measurements. Unpaired, two-tailed Student's t-tests were performed to evaluate statistical significance. P values less than 0.05 were considered statistically significant.

2.9. IACUC

All animal protocols follow the NIH guidelines for animal care and use of laboratory animals (NIH Publication # 85-23 Rev. 1985) and were approved by the University of North Carolina at Chapel Hill Institutional Animal Care and Use Committee.

3. Results and discussion

3.1. Peptide synthesis and ^{64}Cu − labeling

We have prepared four different peptide derivatives for noninvasive visualization and assessment of tumor vasculature, NOTA-FHT, NOTA-(FHT)2, NOTA-PEG-FHT, NOTA-PEG-(FHT)2, utilizing the FHT-peptide as the targeting moiety. All peptide-chelates were assembled on a solid phase peptide synthesizer on a Rink Amide-ChemMatrix resin and were designed to have the chelator NOTA attached to a side chain of a C-terminal Lys residue. A hydrophilic Gly-Gly-Gly-Ser (GGGS) spacer was inserted between the C-terminal end of the FHT-peptide and Lys(NOTA) to allow structural flexibility for optimal in vivo kinetics and high tumor uptake. Additionally two of the constructs, NOTA-PEG-FHT and NOTA-PEG-(FHT)2, had a monodispersed PEG (n = 12 MW600) moiety to modify kinetic properties in vivo. Dimeric peptides were built by adding a Lys-residue and peptide chains were grown from both amino groups of this Lys-residue. The chemical structures of the FHT-peptide and its derivatives are presented in Fig. 1. All four compounds were synthesized in milligram amounts. The chemical identity of the newly synthesized peptide compositions was confirmed by MALDI-TOF mass spectrometry analysis. The HPLC retention time, the experimental MALDI m/z values together with the chemical formula and the calculated theoretical mass for each

compound are listed in Table 1.

Radiolabeling of each ligand was performed at pH 5.5 in 0.1 M ammonium acetate buffer at 50 °C for 30 min. Crude reaction products were purified on a pre-conditioned Sep-Pack light C18 cartridge. Radiochemical yields were greater than 95% and the specific activity was in the range 10–30 MBq/nmol. Each radiopeptide was formulated to pH 7.2 in PBS and filter sterilized before injecting into mice.

3.2. Small animal PET/CT imaging

In vivo noninvasive small animal PET/CT imaging with ^{64}Cu-NOTA-FHT, ^{64}Cu-NOTA-(FHT)2, ^{64}Cu-NOTA-PEG-FHT, and ^{64}Cu-NOTA-PEG-(FHT)2 was conducted in LLC subcutaneous tumor-bearing C57BL/6 immunocompetent mice. In our previous library screening experiments the same immunocompetent mouse model was utilized to select the high affinity FHT-sequence that binds with high specificity to bone marrow-derived tumor vasculature [14]. Discovery and development of new targeting diagnostic and therapeutic peptide sequences in vivo in mice with an intact immune system ensures that the novel peptide-based biomaterial compositions have the desired pharmacokinetic and recognition properties to overcome immune response, which is important for future clinical translation.

Representative decay-corrected transverse small animal PET/CT images acquired at 1 h, 4 h, and 24 h after injection of ^{64}Cu-NOTA-FHT, ^{64}Cu-NOTA-(FHT)2, ^{64}Cu-NOTA-PEG-FHT, and ^{64}Cu-NOTA-PEG-(FHT)2 are displayed in Fig. 2A. Quantitative radioactivity data derived from the microPET/CT analysis for each FHT-composition at 1 h, 4 h, and 24 h p.i. expressed as %ID/g are summarized in Fig. 2B, C and Table 2. Tumor-to-normal tissue ratio comparisons for all four FHT-derivatives are presented in Fig. 3. It is seen from the data that renal clearance is the main route of elimination from the body for all radiopeptides with kidneys presenting the highest uptake of radioactivity with respect to other organs at every time point. All four compounds had low liver uptake at 1 h p.i. (1.10 ± 0.61%ID/g for ^{64}Cu-NOTA-FHT, 1.89 ± 1.30%ID/g for ^{64}Cu-NOTA-(FHT)2, 2.52 ± 0.59%ID/g for ^{64}Cu-NOTA-PEG-FHT, and 5.09 ± 0.06%ID/g for ^{64}Cu-NOTA-PEG-(FHT)2) that stayed constantly low at all time points. Low liver uptake points to the ^{64}Cu-NOTA complex being highly stable in vivo. All four compounds quickly cleared from the blood pool (0.43 ± 0.12%ID/g for ^{64}Cu-NOTA-FHT, 1.25 ± 0.47%ID/g for ^{64}Cu-NOTA-(FHT)2, 1.82 ± 0.17%ID/g for ^{64}Cu-NOTA-PEG-FHT, and 2.35 ± 0.67%ID/g for ^{64}Cu-NOTA-PEG-(FHT)2 at 1 h p.i.) with no residual or persistent radioactivity confirming high chemical inertness and stability of the ^{64}Cu-NOTA complex in vivo.

The highest tumor uptake and retention was observed for ^{64}Cu-NOTA-PEG-(FHT)2 (7.93 ± 1.79%ID/g at 1 h p.i., 4.42 ± 0.45%ID/g at 4 h p.i., and 5.05 ± 1.20%ID/g at 24 h p.i.). However, ^{64}Cu-NOTA-PEG-(FHT)2 demonstrated the highest kidney uptake as well (30.42 ± 2.22%ID/g at 1 h p.i., 29.70 ± 1.22%ID/g at 4 h p.i., and 17.64 ± 1.16%ID/g at 24 h p.i.). At any time point examined the tumor uptake followed the order: ^{64}Cu-NOTA-PEG-(FHT)2 > ^{64}Cu-NOTA-PEG-FHT > ^{64}Cu-NOTA-(FHT)2 > ^{64}Cu-NOTA-FHT. Although ^{64}Cu-NOTA-FHT showed only moderate uptake in tumor (2.01 ± 0.03%ID/g at 1 h p.i., 1.76 ± 0.07%ID/g at 4 h p.i., and 1.72 ± 0.51%ID/g at 24 h p.i.) this compound had faster renal clearance than the rest of the agents studied and cleared from the kidneys and normal organs as early as 1 h p.i. generating high tumor-to-normal tissue ratios (Fig. 3). ^{64}Cu-NOTA-FHT produced reasonable tumor-to-liver and tumor-to-kidney ratios (tumor-to-liver ratio was 1.42 ± 0.25 at 1 h p.i., 2.02 ± 0.17 at 4 h p.i., and 3.40 ± 0.26 at 24 h p.i.; tumor-to-kidney ratio was 0.65 ± 0.03 at 1 h p.i., 0.81 ± 0.13 at 4 h p.i., and 3.49 ± 1.23 at 24 h p.i.) and high tumor-to-blood (3.22 ± 1.35 at 1 h p.i., 4.87 ± 0.64 at 4 h p.i., and 39.33 ± 8.14 at 24 h p.i.) and tumor-to-muscle ratios (17.03 ± 7.41 at 1 h p.i., 24.33 ± 2.66 at 4 h p.i., and 438.79 ± 10.22 at 24 h p.i.). Moreover, tumor-to-normal tissue ratios for ^{64}Cu-NOTA-FHT increased with time thereby enabling improved image contrast. Although ^{64}Cu-NOTA-PEG-(FHT)2 demonstrated enhanced tumor binding and effective avidity, the major increased renal uptake and retention is of concern. The specific cause and mechanism involved in trapping ^{64}Cu-NOTA-PEG-(FHT)2 in the kidneys is not presently known. In general processes of glomerular filtration (i.e., endocytosis) and readsorption in the proximal tubules (i.e., lysosomal metabolism) play a key role in kidney uptake and retention. Urine analysis may reveal the degradation profile of this tracer and identify the metabolites accumulating within the kidneys. Trapping the ^{64}Cu-NOTA-PEG-(FHT)2 agent or its metabolites in the tubular cells and subsequent inefficient excression in the urine creates a radiation burden to the kidneys and ultimately limits the ^{64}Cu-NOTA-PEG-(FHT)2 activity that can be administered safely into a patient (see also radiation absorbed dose discussion in Section 3.4).

Generally in evaluating new tumor imaging agents while the accumulation of the agent in the tumor is important it is not the absolute uptake but the contrast between target-to-non-target tissue that defines the utility of the imaging agent and determines its potential for clinical translation [21]. Within this context the microPET/CT imaging studies revealed that out of the four compounds studied ^{64}Cu-NOTA-FHT possesses most favorable pharmacokinetics with rapid clearance from normal tissues including the kidney and hence ^{64}Cu-NOTA-FHT was selected for further characterization.

To ensure that ^{64}Cu-NOTA-FHT accumulates in the tumor due to specific binding of the FHT-peptide to its cellular target, ^{64}Cu-NOTA-FHT was tested for binding specificity by imaging a mouse that was administered a mixture of radiolabeled and unlabeled peptide (20 mg/kg) ($n = 3$). The unlabeled peptide proved capable of significantly reducing tumor uptake of the radiolabeled counterpart (without blocking 2.01 ± 0.03%ID/g; with blocking 0.80 ± 0.27%ID/g, $p = 0.005$) (Fig. 4). Furthermore uptake in normal organs under blocking conditions was similar. These data demonstrate that the observed accumulation of radioactivity in the tumor is peptide -mediated.

3.3. Rodent biodistribution studies

Biodistribution of ^{64}Cu-NOTA-FHT was studied in female C67BL/6 mice bearing s.c. LLC tumors. Biodistribution data collected at 1 h, 4 h, and 24 h after ^{64}Cu-NOTA-FHT injection are presented in Fig. 5A

Table 1
Analytical data for the newly synthesized FHT-derivatives.

Peptide derivative	Retention time, min	Experimental $[M+H]^+$	Chemical formula	Molecular mass (theoretical)
NOTA-FHT	7.84	2240.1[a]	$C_{98}H_{146}N_{30}O_{29}S$	2240.49
NOTA-(FHT)2	6.14	4014	$C_{176}H_{263}N_{55}O_{52}S$	4013.43
NOTA-PEG-FHT	6.79	2839.5[a]	$C_{125}H_{199}N_{31}O_{42}S$	2840.20
NOTA-PEG-(FHT)2	7.24	4613	$C_{203}H_{316}N_{56}O_{65}S$	4613.15

[a] Monoisotopic $[M+H]^+$ (isotopic peaks resolved).

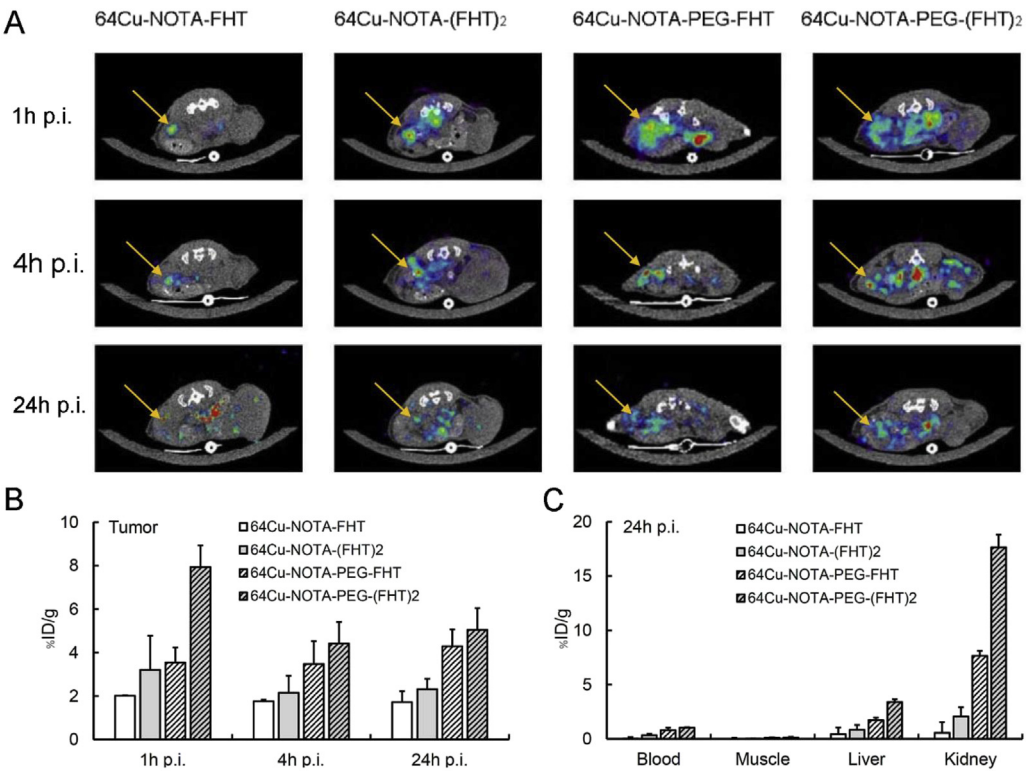

Fig. 2. (A) Representative decay-corrected transverse microPET/CT images of ^{64}Cu-NOTA-FHT, ^{64}Cu-NOTA-(FHT)2, ^{64}Cu-NOTA-PEG-FHT, and ^{64}Cu-NOTA-PEG-(FHT)2 at 1 h, 4 h, and 24 h after injection in LLC tumors subcutaneously implanted in the right inguinal region. Tumors are indicated by orange arrow. (B) Comparative tumor uptake, %ID/g, of ^{64}Cu-NOTA-FHT (white bars), ^{64}Cu-NOTA-(FHT)2 (gray bars), ^{64}Cu-NOTA-PEG-FHT (white patterned bars), and ^{64}Cu-NOTA-PEG-(FHT)2 (gray patterned bars) at 1 h, 4 h, and 24 h p.i. (C) Uptake of ^{64}Cu-NOTA-FHT, ^{64}Cu-NOTA-(FHT)2, ^{64}Cu-NOTA-PEG-FHT, and ^{64}Cu-NOTA-PEG-(FHT)2 in other organs of interest at 24 h p.i. Data are presented as mean %ID/g ± SD (n = 3). (For interpretation of the references to color in this figure legend, the reader is referred to the web version of this article.)

Table 2
Uptake of ^{64}Cu-NOTA-FHT, ^{64}Cu-NOTA-(FHT)2, ^{64}Cu-NOTA-PEG-FHT, and ^{64}Cu-NOTA-PEG-(FHT)2 at 1 h p.i., 4 h p.i., and 24 h p.i. in blood, muscle, liver, kidney, and tumor of s.c. LLC-tumor bearing mice determined by quantitative PET image analysis expressed as mean %ID/g ± SD (n = 3).

FHT-radiopeptide/tissue	1 h p.i.	4 h p.i.	24 h p.i.
64Cu-NOTA-FHT			
Tumor	2.01 ± 0.03	1.76 ± 0.07	1.72 ± 0.51
Blood	0.43 ± 0.12	0.39 ± 0.02	0.04 ± 0.00
Muscle	0.16 ± 0.10	0.07 ± 0.06	0.00 ± 0.00
Liver	1.10 ± 0.61	0.69 ± 0.39	0.44 ± 0.27
Kidney	2.27 ± 0.98	1.61 ± 0.74	0.57 ± 0.32
64Cu-NOTA-(FHT)2			
Tumor	3.20 ± 1.58	2.15 ± 0.78	2.32 ± 0.47
Blood	1.25 ± 0.47	0.85 ± 0.54	0.35 ± 0.13
Muscle	0.27 ± 0.11	0.12 ± 0.09	0.04 ± 0.01
Liver	1.89 ± 1.30	1.48 ± 0.91	0.84 ± 0.44
Kidney	5.06 ± 2.32	4.62 ± 1.82	2.07 ± 0.84
64Cu-NOTA-PEG-FHT			
Tumor	3.54 ± 0.69	3.48 ± 1.05	4.29 ± 0.78
Blood	1.82 ± 0.17	1.34 ± 0.23	0.8 ± 0.24
Muscle	0.32 ± 0.03	0.19 ± 0.03	0.11 ± 0.03
Liver	2.52 ± 0.59	2.57 ± 0.59	1.74 ± 0.23
Kidney	23.9 ± 4.68	18.51 ± 2.09	7.67 ± 0.44
64Cu-NOTA-PEG-(FHT)2			
Tumor	7.93 ± 1.79	4.42 ± 0.45	5.05 ± 1.20
Blood	2.35 ± 0.67	2.33 ± 0.21	1.04 ± 0.04
Muscle	1.15 ± 0.29	0.41 ± 0.02	0.13 ± 0.06
Liver	5.09 ± 0.06	4.54 ± 0.27	3.39 ± 0.27
Kidney	30.42 ± 2.22	29.7 ± 1.22	17.64 ± 1.16

and Table 1 in Ref. [37]. It is seen from the figure that ^{64}Cu-NOTA-FHT radioactivity is cleared quickly from the blood pool, muscle, liver, spleen, kidney, lungs, heart, stomach, small intestine, large intestine, bone, thyroid, and pancreas. The highest uptake at 1 h p.i. occurred in the kidneys (5.08 ± 0.84%ID/g), followed by lungs (2.00 ± 0.19%ID/g) and liver (1.63 ± 0.24%ID/g). However, kidney, lungs, and liver radioactivity cleared rapidly. Moreover, little to no ^{64}Cu-FHT-NOTA bone uptake was observed over time. This low bone activity background may proof useful in enabling enhanced contrast for detecting metastatic spreads which in many tumor types are primarily found in bone. The radioactivity of the tumor was reasonable and persisted up to 24 h p.i. (0.42 ± 0.03%ID/g at 1 h p.i., 0.43 ± 0.22%ID/g at 4 h p.i., and 0.37 ± 0.08%ID/g at 24 h p.i.) confirming the findings from the microPET/CT imaging.

A separate blocking study was conducted at 1 h after injection of a mixture of ^{64}Cu-NOTA-FHT and excess of unlabeled NOTA-FHT (20 mg/kg) (n = 3). Biodistribution of ^{64}Cu-NOTA-FHT under blocking conditions is shown in Fig. 5B. Cumulative tumor uptake in the presence of NOTA-FHT showed small but significant decrease (without blocking 0.42 ± 0.03%ID/g; with blocking 0.31 ± 0.06%ID/g, p = 0.032). These observations indicate that radioactivity accumulation in the tumor is mediated by the FHT-peptide. Under blocking conditions radioactivity uptake in normal organs was unchanged. This was expected since the expression of the target for the FHT-peptide is restricted to bone marrow-derived tumor vasculature. Biodistribution results are consistent with the findings from the microPET/CT studies for ^{64}Cu-FHT-NOTA and confirm the unique targeting specificity of the FHT-sequence both on a molecular and tissue level.

During the last decade extensive work has been undertaken on the development of ^{64}Cu-labeled radiopeptides [6,9,17,18,21,38–40]. Most molecular imaging studies utilize the

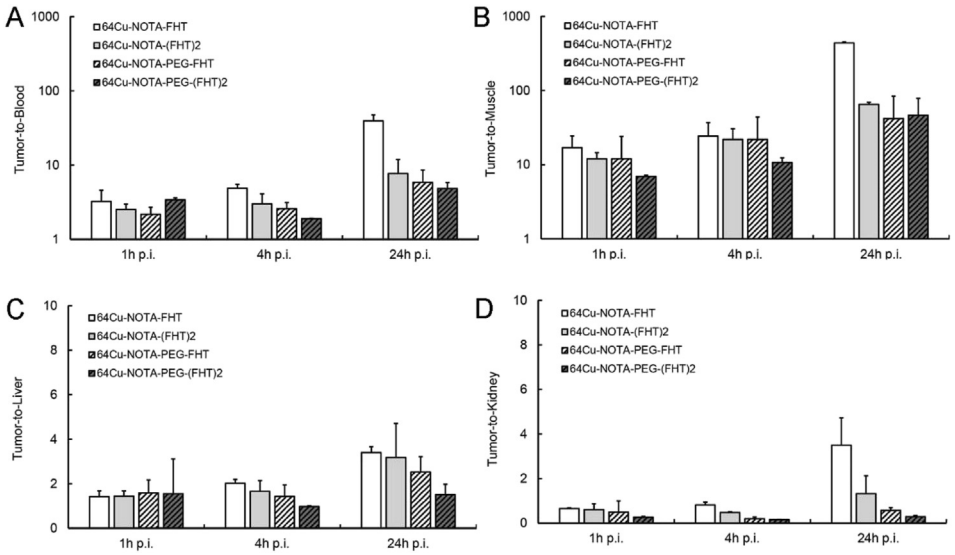

Fig. 3. (A) Tumor-to-blood, (B) tumor-to-muscle, (C) tumor-to-liver, and (D) tumor-to-kidney ratios determined from the microPET/CT images for ^{64}Cu-NOTA-FHT (white bars), ^{64}Cu-NOTA-(FHT)2 (gray bars), ^{64}Cu-NOTA-PEG-FHT (white patterned bars), and ^{64}Cu-NOTA-PEG-(FHT)2 (gray patterned bars) in LLC tumor bearing mice. The y-axis on panels (A) and (B) is in logarithmic scale. Tumor-to-normal organ ratios for ^{64}Cu-NOTA-FHT are notably higher (n = 3).

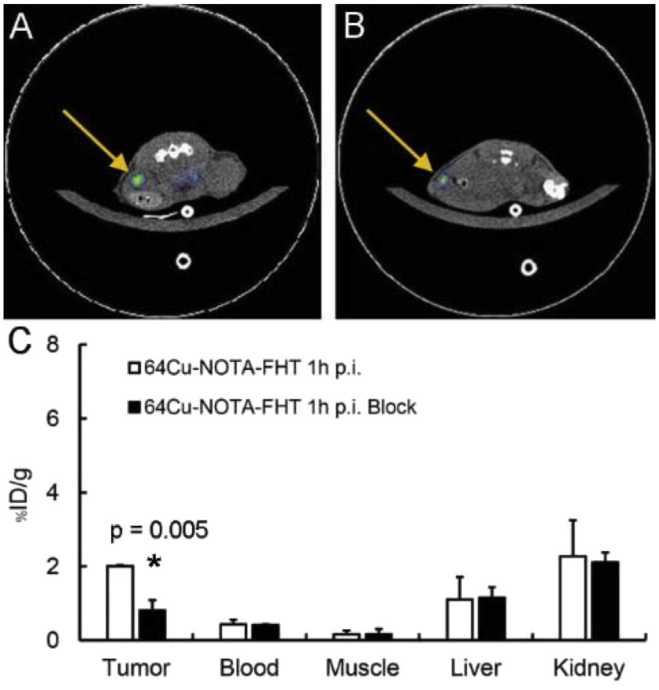

Fig. 4. Representative decay-corrected transverse microPET/CT images in LLC tumor-bearing mice (tumors are indicated by arrows). (A) 1 h after injection of ^{64}Cu-NOTA-FHT; (B) 1 h after co-injection of ^{64}Cu-NOTA-FHT and unlabeled NOTA-FHT blocking dose. (C) Uptake in tumor, blood, muscle, liver, and kidney obtained from quantitative analysis of the microPET/CT images. Tumor uptake of ^{64}Cu-NOTA-FHT is significantly reduced in the presence of NOTA-FHT (p = 0.005) indicating specific, FHT-mediated tumor accumulation (n = 3).

Arg-Gly-Asp sequence of several extracellular matrix proteins, as the lead structure to grant specificity to integrin receptors which are overexpressed both on tumor vasculature and tumor cells. Various design approaches to optimize the lead RGD vector for improved pharmacokinetics and tumor accumulation have been devised in a variety of tumor bearing mouse models. Dumont et al. [39] developed a ^{64}Cu-RGD conjugate as an attractive alternative to ^{18}F-labeled RGD tracer with improved tumor-to-background ratios. Another strategy to target cellular integrin receptors is the utilization of the knottin peptide [40]. Nielsen et al. prepared the ^{64}Cu-DOTA-knottin tracer and conducted head-to-head comparison with FDG in a transgenic mouse model of lung cancer. ^{64}Cu-DOTA-knottin 2.5F tracer produced statistically higher tumor-to background rations compared to FDG. Although our findings are not directly comparable to those reported in the literature due to different chelation chemistries, target vector modifications, and different tumor models, a distinct feature of the ^{64}Cu-NOTA-FHT imaging tracer developed here is dramatically improved contrast due to higher tumor-to-background ratios. The FHT-radiopeptide binds specifically to its target with high affinity in vivo and is retained in the tumor vasculature. At the same time it clears quickly from normal tissue. This fast clearance is expected to limit the absorbed dose to healthy tissues in humans as discussed in the next section.

3.4. Dosimetry calculations

^{64}Cu-NOTA-FHT human absorbed dose estimates were based on the biodistribution of the radiopeptide in C57BL/6 mice at 1 h p.i., 4 h p.i., and 24 h p.i. Activity trapped in an organ after 24 h was considered to be cleared only by physical decay of ^{64}Cu. Further, the assumption was made that the mouse distribution determined at various time points is the same as the human distribution (for detailed analysis see Ref. [37]). The radiation absorbed doses in liver, spleen, kidney, lungs, stomach, small and large intestines, thyroid and pancreas in mGy per MBq of injected ^{64}Cu-NOTA-FHT radioactivity are summarized in Table 3. Based on these data kidneys are the dose-limiting organ with an average radiation dose 0.191 mGy/MBq. The relatively small absorbed dose to the normal organs allows for the safe injection of 500–800 MBq which is sufficient for clinical PET imaging. Because of its favorable dosimetry profile ^{64}Cu-NOTA-FHT appears very promising for clinical translation.

4. Conclusions

We report on the synthesis and characterization of four new

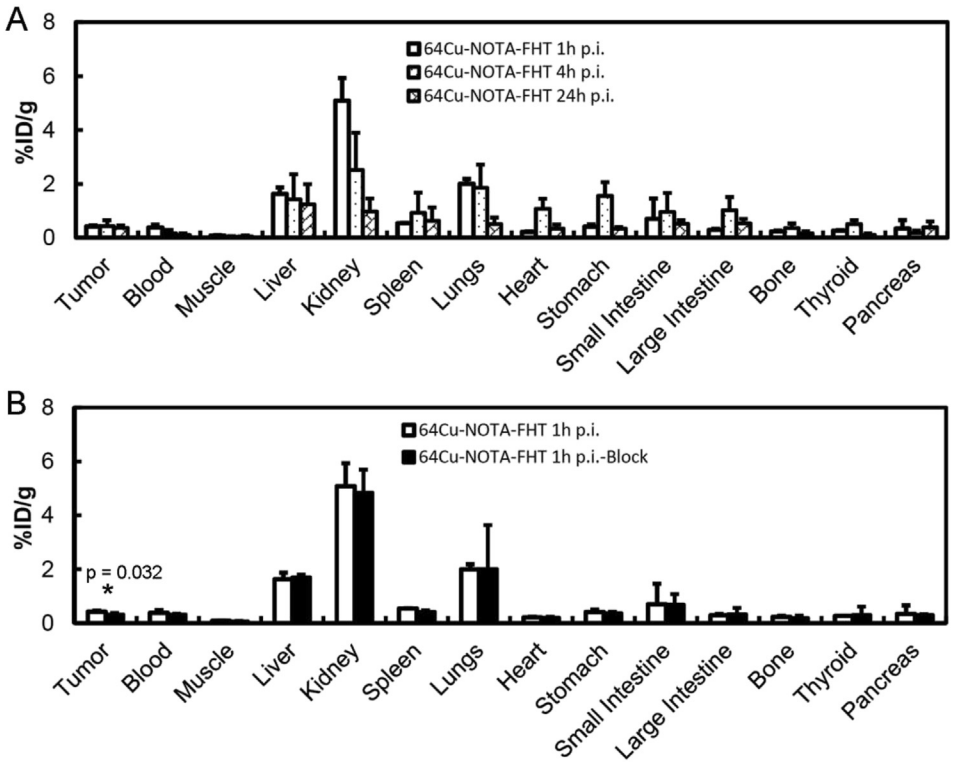

Fig. 5. (A) ^{64}Cu-NOTA-FHT biodistribution in the tumor and normal organs in LLC tumor bearing C57BL/6 mice at 1 h p.i., 4 h p.i., and 24 h p.i. (B) ^{64}Cu-NOTA-FHT biodistribution in the tumor and normal organs in LLC tumor bearing C57BL/6 mice at 1 h p.i. in the presence of unlabeled NOTA-FHT (20 mg/kg). Small but significant decrease in accumulation of ^{64}Cu-NOTA-FHT in tumor but not in other organs in the presence of NOTA-FHT blocking dose points to specific tumor targeting enabled by the FHT-peptide ($p = 0.032$) ($n = 3$).

Table 3
Human radiation absorbed dose estimates (in mGy per MBq) resulting from administration of ^{64}Cu-NOTA-FHT extrapolated from mouse distribution data using the MIRD S-values [36].

Tissue	Radiation absorbed dose, mGy/MBq
Liver	1.56E-02 ± 2.59E-03
Spleen	1.08E-03 ± 7.26E-05
Kidney	1.91E-01 ± 1.35E-02
Lungs	4.51E-03 ± 3.09E-04
Stomach	7.63E-03 ± 1.89E-04
Small intestine	6.68E-03 ± 8.49E-04
Large intestine	1.20E-02 ± 4.14E-03
Thyroid	1.02E-01 ± 8.87E-03
Pancreas	1.76E-02 ± 3.67E-03

^{64}Cu-labeled peptide compositions for PET imaging of tumor vasculature that all incorporate the phage display-selected high affinity, cell-specific FHT-peptide. Our results reveal that the ^{64}Cu-NOTA-FHT derivative demonstrates superior pharmacokinetic properties with rapid clearance from normal tissues including the kidneys resulting in high tumor-to-normal tissue ratios and improved image contrast. Further, our studies indicate that the unique imaging contrast is specifically enabled by the FHT-peptide. The low absorbed dose ^{64}Cu-NOTA-FHT profile highlights potential clinical utility. Further development of ^{64}Cu-NOTA-FHT as novel targeted radiopharmaceutical for diagnostic PET imaging of aggressive tumor vasculature is warranted.

Acknowledgments

Research presented in this publication was supported by the National Science Foundation with Award No: 1321424.

References

[1] D.F. Williams, On the nature of biomaterials, Biomaterials 30 (2009) 5897–5909.
[2] D. Williams, Essential materials science, Essent. Biomater. Sci. (2014) 29–128.
[3] A.N. Veleva, D.E. Heath, S.L. Cooper, C. Patterson, Selective endothelial cell attachment to peptide-modified terpolymers, Biomaterials 29 (2008) 3656–3661.
[4] T.A. Petrie, J.E. Raynor, C.D. Reyes, K.L. Burns, D.M. Collard, A.J. Garcia, The effect of integrin-specific bioactive coatings on tissue healing and implant osseointegration, Biomaterials 29 (2008) 2849–2857.
[5] U. Hersel, C. Dahmen, H. Kessler, RGD modified polymers: biomaterials for stimulated cell adhesion and beyond, Biomaterials 24 (2003) 4385–4415.
[6] C.M. Kang, H.J. Koo, G.I. An, Y.S. Choe, J.Y. Choi, K.H. Lee, B.T. Kim, Hybrid PET/optical imaging of integrin alpha(V)beta(3) receptor expression using a Cu-64-labeled streptavidin/biotin-based dimeric RGD peptide, EJNMMI Res. 5 (2015).
[7] K.G. Li, Z.L. Zhang, L.F. Zheng, H. Liu, W. Wei, Z.Y. Li, Z.Y. He, A.C. Larson, G.X. Zhang, Arg-Gly-Asp-D-Phe-Lys peptide-modified PEGylated dendrimer-entrapped gold nanoparticles for targeted computed tomography imaging of breast carcinoma, Nanomedicine 10 (14) (2015) 2185–2197.
[8] G.J. Yang, P. Nie, Y. Kong, H.K. Sun, G.H. Hou, J.K. Han, MicroPET imaging of tumor angiogenesis and monitoring on antiangiogenic therapy with an F-18 labeled RGD-based probe in SKOV-3 xenograft-bearing mice, Tumor Biol. 36 (5) (2015) 3285–3291.
[9] X.Y. Chen, Y.P. Hou, M. Tohme, R. Park, V. Khankaldyyan, I. Gonzales-Gomez, J.R. Bading, W.E. Laug, P.S. Conti, Pegylated Arg-Gly-Asp peptide: Cu-64 labeling and PET imaging of brain tumor alpha(v)beta(3)-integrin expression, J. Nucl. Med. 45 (10) (2004) 1776–1783.
[10] E.N. Peletskaya, V.V. Glinsky, G.V. Glinsky, S.L. Deutscher, T.P. Quinn, Characterization of peptides that bind the tumor-associated Thomsen-Friedenreich antigen selected from bacteriophage display libraries, J. Mol. Biol. 270 (1997) 374–384.
[11] T. Oyama, K.F. Sykes, K.N. Samli, J.D. Minna, S.A. Johnston, K.C. Brown, Isolation of lung tumor specific peptides from a random peptide library: generation of diagnostic and cell-targeting reagents, Cancer Lett. 202 (2003) 219–230.
[12] M. Koolpe, R. Burgess, M. Dail, E.B. Pasquale, EphB receptor-binding peptides identified by phage display enable design of an antagonist with ephrin-like affinity, J. Biol. Chem. 280 (2005) 17301–17311.
[13] A.N. Veleva, S.L. Cooper, C. Patterson, Selection and initial characterization of novel peptide ligands that bind specifically to human blood outgrowth endothelial cells, Biotechnol. Bioeng. 98 (2007) 306–312.
[14] A.N. Veleva, D.B. Nepal, C.B. Frederick, J. Schwab, P. Lockyer, H. Yuan, et al.,

Efficient in vivo selection of a novel tumor-associated peptide from a phage display library, Molecules 16 (2011) 900–914.
[15] S.L. Deutscher, K.A. Kelly, Imaging with bacteriophage-derived probes, Phage Nanobiotechnol. (2011) 83–100.
[16] A.N. Singh, M.J. McGuire, S. Li, G. Hao, A. Kumar, X. Sun, et al., Dimerization of a phage-display selected peptide for imaging of alpha(v)beta(6) - integrin: two approaches to the multivalent effect, Theranostics 4 (2014) 745–760.
[17] S.R. Kumar, F.A. Gallazzi, T.P. Quinn, S.L. Deutscher, Cu-64-labeled peptide for PET of breast carcinomas expressing the Thomsen-Friedenreich carbohydrate antigen, J. Nucl. Med. 52 (2011) 1819–1826.
[18] C. Xiong, M. Huang, R. Zhang, S. Song, W. Lu, L. Flores II, et al., In vivo small-animal PET/CT of EphB4 receptors using Cu-64-labeled peptide, J. Nucl. Med. 52 (2011) 241–248.
[19] C. Patterson, C.B. Frederick, H. Yuan, L.A. Dyer, P. Lockyer, D.S. Lalush, et al., Development of a new positron emission tomography tracer for targeting tumor angiogenesis: synthesis, small animal imaging, and radiation dosimetry, Molecules 18 (2013) 5594–5610.
[20] X.Y. Chen, E. Sievers, Y.P. Hou, R. Park, M. Tohme, R. Bart, et al., Integrin alpha(V)beta(3)-targeted imaging of lung cancer, Neoplasia 7 (2005) 271–279.
[21] S.J. DeNardo, R. Liu, H. Albrecht, A. Natarajan, J.L. Sutcliffe, C. Anderson, et al., (111)In-LLP2A-DOTA polyethylene glycol-targeting alpha 4 beta 1 integrin: comparative pharmacokinetics for imaging and therapy of lymphoid malignancies, J. Nucl. Med. 50 (2009) 625–634.
[22] S. Rafii, D. Lyden, R. Benezra, K. Hattori, B. Heissig, Vascular and haematopoietic stem cells: novel targets for anti-angiogenesis therapy? Nat. Rev. Cancer 2 (2002) 826–835.
[23] D. Lyden, K. Hattori, S. Dias, C. Costa, P. Blaikie, L. Butros, et al., Impaired recruitment of bone-marrow-derived endothelial and hematopoietic precursor cells blocks tumor angiogenesis and growth, Nat. Med. 7 (2001) 1194–1201.
[24] D.G. Duda, K.S. Cohen, S.V. Kozin, J.Y. Perentes, D. Fukumura, D.T. Scadden, et al., Evidence for incorporation of bone marrow-derived endothelial cells into perfused blood vessels in tumors, Blood 107 (2006) 2774–2776.
[25] J. Aitsebaomo, S. Srivastava, H. Zhang, S. Jha, Z. Wang, S. Winnik, et al., Recombinant human interleukin-11 treatment enhances collateral vessel growth after femoral artery ligation, Arterioscler. Thromb. Vasc. Biol. 31 (2011) 306–312.
[26] D. Lyden, K. Hattori, S. Dias, K. Hajjar, K. Manova, M.A.S. Moore, et al., Transplantation of bone marrow derived VEGF-responsive hematopoietic and vasculogenic precursor cells are essential to restore the angiogenic defect in Id1+/-Id3-/- knock out mice, Blood 96 (2000), 529A–A.
[27] H. Zhang, V. Vakil, M. Braunstein, E.L.P. Smith, J. Maroney, L. Chen, et al., Circulating endothelial progenitor cells in multiple myeloma: implications and significance, Blood 105 (2005) 3286–3294.
[28] G. Furstenberger, R. von Moos, R. Lucas, B. Thurlimann, H.J. Senn, J. Hamacher, et al., Circulating endothelial cells and angiogenic serum factors during neoadjuvant chemotherapy of primary breast cancer, Br. J. Cancer 94 (2006) 524–531.
[29] B. Dome, J. Timar, J. Dobos, L. Meszaros, E. Raso, S. Paku, et al., Identification and clinical significance of circulating endothelial progenitor cells in human non-small cell lung cancer, Cancer Res. 66 (2006) 7341–7347.
[30] N. Rafat, G.C. Beck, J. Schulte, J. Tuettenberg, P. Vajkoczy, Circulating endothelial progenitor cells in malignant gliomas clinical article, J. Neurosurg. 112 (2010) 43–49.
[31] J.M. Roodhart, M.H. Langenberg, J.S. Vermaat, M.P. Lolkema, A. Baars, R.H. Giles, et al., Late release of circulating endothelial cells and endothelial progenitor cells after chemotherapy predicts response and survival in cancer patients, Neoplasia 12 (2010) 87–94.
[32] D.G. Duda, K.S. Cohen, E. di Tomaso, A.P. Au, R.J. Klein, D.T. Scadden, et al., Differential CD 146 expression on circulating versus tissue endothelial cells in rectal cancer patients: implications for circulating endothelial and progenitor cells as biomarkers for antiangiogenic therapy, J. Clin. Oncol. 24 (2006) 1449–1453.
[33] B.P. Gray, K.C. Brown, Combinatorial peptide libraries: mining for cell-binding peptides, Chem. Rev. 114 (2014) 1020–1081.
[34] W. Arap, R. Pasqualini, E. Ruoslahti, Cancer treatment by targeted drug delivery to tumor vasculature in a mouse model, Science 279 (5349) (1998) 377–380.
[35] M. Kume, P.C. Carey, G. Gaehle, E. Madrid, T. Voller, W. Margenau, et al., A semi-automated system for the routine production of copper-64, Appl. Radiat. Isotopes 70 (2012) 1803–1806.
[36] W.S. Snyder, M.R. Ford, G.G. Wamer, S.B. Watson, MIRD Pamphlet No. 11, Society of Nuclear Medicine, New York, NY, USA, 1975, pp. 92–93.
[37] J.R. Merrill, K. Krajewski, H. Yuan, J.E. Frank, D.S. Lalush, C. Patterson, A. Veleva, Data on Biodistribution and Radiation Absorbed Dose Profile of a Novel 64Cu-labeled High Affinity Cell-specific Peptide for Positron Emission Tomography Imaging of Tumor Vasculature, Data in Brief, 2016. submitted.
[38] F.C. Gaertner, H. Kessler, H.J. Wester, M. Schwaiger, A.J. Beer, Radiolabelled RGD peptides for imaging and therapy, Eur. J. Nucl. Med. Mol. Imaging 39 (2012) 126–138.
[39] R.A. Dumont, F. Deininger, R. Haubner, H.R. Maecke, W.A. Weber, M. Fani, Novel Cu-64- and Ga-68-labeled RGD conjugates show improved PET imaging of alpha(v)beta(3) integrin expression and facile radiosynthesis, J. Nucl. Med. 52 (8) (2011) 1276–1284.
[40] C.H. Nielsen, R.H. Kimura, N. Withofs, P.T. Tran, Z. Miao, J.R. Cochran, Z. Cheng, D. Felsher, A. Kjaer, J.K. Willmann, S.S. Gambhir, PET imaging of tumor neovascularization in a transgenic mouse model with a novel Cu-64-DOTA-knottin peptide, Cancer Res. 70 (22) (2010) 9022–9030.